

# FOOTPOINT MOTION OF THE CONTINUUM EMISSION IN THE 2002 SEPTEMBER 30 WHITE-LIGHT FLARE

Q. R. Chen and M. D. Ding

*Department of Astronomy, Nanjing University, Nanjing 210093, China*

## ABSTRACT

We present observations of the 2002 September 30 white-light flare, in which the optical continuum emission near the  $H\alpha$  line is enhanced by  $\sim 10\%$ . The continuum emission exhibits a close temporal and spatial coincidence with the hard X-ray (HXR) footpoint observed by *RHESSI*. We find a systematic motion of the flare footpoint seen in the continuum emission; the motion history follows roughly that of the HXR source. This gives strong evidence the this white-light flare is powered by heating of nonthermal electrons. We note that the HXR spectrum in 10–50 keV is quite soft with  $\gamma \approx 7$  and there is no HXR emission above 50 keV. The magnetic configuration of the flaring region implies magnetic reconnection taking place at a relatively low altitude during the flare. Despite a very soft spectrum of the electron beam, its energy content is still sufficient to produce the heating in the lower atmosphere where the continuum emission originates. This white-light flare highlights the importance of radiative backwarming to transport the energy below when direct heating by beam electrons is obviously impossible.

*Subject headings:* Sun: flares — Sun: magnetic fields — Sun: X-rays, gamma rays

## 1. INTRODUCTION

Compared to ordinary solar flares, white-light flares (WLFs) manifest themselves with an enhanced emission in the optical continuum of a few or tens of percent, or even more in some extreme cases. The continuum emission originates in the lower chromosphere and below. Therefore, research on WLFs can reveal critical clues to energy transport and heating mechanisms in the solar lower atmosphere (Neidig 1989; Ding, Fang, & Yun 1999).

Most of the WLFs observed so far belong to Type I WLFS that are spectrally characterized with a Balmer and Paschen jump and strong broadened hydrogen Balmer lines (Machado et al. 1986). Observations usually demonstrate a close temporal correspondence between the continuum and the hard X-ray (HXR) emissions in these WLFS (e.g., Hudson et al. 1992; Fang & Ding 1995; Neidig & Kane 1993; Matthews et al. 2003; Metcalf et al. 2003; Hudson, Wolfson, & Metcalf 2005). This implies that the continuum emission is closely related to nonthermal heating of energetic electrons, which are assumed to be accelerated in the corona and then stream downward to the chromosphere. However, this process alone, in most cases, cannot efficiently produce the continuum emission since very few electrons ( $E \geq 200$  keV) can penetrate to the lower chromosphere and below (Ding et al. 2003b). Therefore, radiative backwarming is further invoked to transfer the enhanced chromospheric radiation to deeper layers to produce the heating there and finally an enhanced continuum emission (Hudson 1972; Aboudarham & Hénoux 1987; Machado, Emslie, & Avrett 1989; Metcalf et al. 1990a; Metcalf, Canfield, & Saba 1990b; Gan & Mauas 1994; Ding et al. 2003b). A recent radiative hydrodynamic model of solar flares, which includes the electron beam heating and radiative transport in a consistent way, reproduces the continuum enhancement comparable to the observed values (Allred et al. 2005). On the other hand, observations show that in some few very energetic events, electrons can be accelerated to very high energies, e.g., 300–800 keV (Xu et al. 2004, 2005). In such cases, a large amount of nonthermal electrons can penetrate deep into the atmosphere, and direct collisional heating may play an important role in producing the continuum emission.

It has been widely accepted that nonthermal electrons, accelerated by magnetic reconnection in the corona, stream downward along magnetic fields and produce the HXR emission in the chromosphere via bremsstrahlung radiation (Brown 1971). According to this scenario, the apparent motions of HXR sources reflect the successive reconnection process between neighboring field lines in the corona (e.g., Qiu et al. 2002). Observations of footpoint motions can thus provide a test or constraint on theoretical models of solar flares. There are, up to now, quite some observations revealing the motions of HXR sources indicative of successive reconnection under various magnetic topologies (e.g., Sakao et al. 2000; Krucker, Hurford, & Lin 2003). However, few examples have shown the motions of white-light continuum kernels that are related with the HXR sources.

In this paper, we present observations of a white-light flare on 2002 September 30. We examine the temporal and spatial relationship between the continuum emission and the HXR emission during the flare and discuss its energetics. In particular, We discover a fairly good

correlation between the motion history of the white-light kernel and the corresponding HXR source. We explain the observed continuum emission in terms of nonthermal heating by electron beams followed by the radiative backwarming effect.

## 2. OBSERVATIONS AND DATA ANALYSIS

According to the Solar-Geophysical Data, the flare of 2002 September 30 is an M2.1/1B event that occurred in NOAA Active Region 0134 ( $N13^\circ$ ,  $E10^\circ$ ). The profiles of *GOES* soft X-ray (SXR) fluxes show that the flare began at  $\sim$ 01:44 UT and peaked at  $\sim$ 01:50 UT. The hard X-ray (HXR) emission up to 50 keV of this flare was observed by the *Reuven Ramaty High-Energy Solar Spectroscopic Imager (RHESSI)*, which provides unprecedented high resolution imaging and spectroscopy capacity for solar flares (Lin et al. 2002). Note that this flare and the M2.6/2B flare on 2002 September 29 (Ding et al. 2003a; Chen & Ding 2005) are two homologous flares in the same active region.

Using the imaging spectrograph of the Solar Tower Telescope of Nanjing University (Huang et al. 1995) and employing a scanning technique, we obtained a sequence of two-dimensional spectra of the H $\alpha$  and Ca II 8542 Å lines across the whole flaring region at a time cadence of  $\sim$ 15 s. There are 120 pixels with a spacing of 0''.85 along the slit and 50 steps with a spacing of 2'' along the scanning direction. The spectra contain 260 wavelength pixels with a resolution of 0.05 Å and 0.118 Å for the H $\alpha$  and Ca II 8542 Å lines, and thus span a range of about 13 Å and 30 Å, respectively.

During the flare, the line widths of the H $\alpha$  and Ca II 8542 Å lines increase gradually and then decrease after the maximum phase; the peak values of FWHM are about 4.5 Å and 1.5 Å, respectively. We extract a narrow window in the far red wing of the H $\alpha$  line (e.g.,  $\Delta\lambda = 6$  Å) and use it as a proxy of the nearby continuum. We check carefully the line profiles and ensure that the line emission has little influence on the continuum window. We define the continuum contrast as  $(I_f - I_q)/I_q$ , where  $I_f$  is the flare intensity and  $I_q$  the preflare background (taken about one hour before the flare) at the same point. By checking the mean intensity fluctuation outside the flaring region, we further estimate the measurement error of the continuum contrast to be below 1%.

Reduction of ground-based data includes dark field and flat field corrections. We coalign the H $\alpha$  images in line wings with the *Solar and Heliospheric Observatory* MDI continuum images (Scherrer et al. 1995) by correlating the sunspot features. The accuracy of image

coalignment is estimated to be  $\sim 2''$ .

### 3. RESULTS AND DISCUSSIONS

#### 3.1. ENERGETICS OF THE CONTINUUM EMISSION

We present in Figure 1 a sequence of images of this flare as seen in the  $\text{H}\alpha$  line center (*gray scale*), the continuum ( $\text{H}\alpha + 6 \text{ \AA}$ , *white contours*), and *RHESSI* 12–25 keV HXR (*black contours*). HXR images are reconstructed with the CLEAN algorithm from detectors 3–8, which yields an angular resolution of  $\sim 7''$ . Note that the flare is located near the solar disk center and the flaring loops are very compact. Therefore, the  $\text{H}\alpha$  or HXR emission from the loop top and the footpoints may probably be spatially mixed together due to projection effect. We also select a 171  $\text{\AA}$  EUV image from the *Transition Region and Coronal Explorer* (*TRACE*, Handy et al. 1999) to show the large structure of the flaring region.

We investigate the origin of the continuum emission by examining its relationship with the HXR emission during the flare, which provides important information about the heating processes in the flaring atmosphere. As seen in Figure 1, the flare has a simple compact morphology in the continuum and the HXR emission, both of which reside at the main  $\text{H}\alpha$  ribbon; there is a close spatial coincidence between the continuum and the HXR emission. We also examine the temporal variation of the continuum contrast at the position denoted with the *plus* sign in Figure 1 where the maximum continuum contrast appears during the flare. As seen in Figure 2, the continuum contrast reaches a maximum of  $\sim 10\%$  at  $\sim 01:49:17$  UT and correlates well with the HXR emission during the flare.<sup>1</sup> Note that for this flare, the time profiles for the HXR emission below 50 keV are rather gradual and there is no HXR emission above 50 keV. Observations from the solar broad-band *Hard X-Ray Spectrometer* (*HXRS*, Fárník, García, & Karlický 2001) give similar results. The close temporal and spatial relationship between the continuum and HXR emission in this flare indicates that the continuum emission is strongly related to nonthermal energy deposition in the chromosphere.

Current WLF models have proposed electron beam heating plus the radiative back-

---

<sup>1</sup>In the far blue wing of the  $\text{H}\alpha$  line ( $\Delta\lambda = -6 \text{ \AA}$ ), the continuum develops similarly and reaches a maximum contrast of  $\sim 8\%$ . In a near-infrared window near the  $\text{Ca II}$  8542  $\text{\AA}$  line, we detect a much lower contrast of the continuum ( $\sim 2\%$ ).

warming effect to account for the observed continuum enhancement. Ding et al. (2003b) and Chen & Ding (2005) calculated the continuum contrast near the CaII 8542 Å and the H $\alpha$  lines, respectively, as a function of the energy flux of the electron beam impacting a model atmosphere.

For this flare, we can apply a single power-law fitting to the photon spectrum for the HXR source during the maximum phase, as seen in Figure 3. The power-law spectrum extends down to  $\sim$ 10 keV and has an index of  $\gamma = 7.4$ , which is much larger than the often observed values, e.g., 3–5. In the scenario that the above HXR emission is produced via thick-target bremsstrahlung (Brown 1971) by nonthermal electrons with an assumed low-energy cutoff of 20 keV, the nonthermal electron power is derived to be  $\sim 3 \times 10^{28}$  ergs s $^{-1}$  and the energy flux ( $F_{20}$ ) is estimated to be  $\sim 2.0 \times 10^{10}$  ergs cm $^{-2}$  s $^{-1}$  (an average value from 01:49:00 to 01:50:00 UT). According to Chen & Ding (2005), an energy flux of  $\sim 2.0 \times 10^{10}$  ergs cm $^{-2}$  s $^{-1}$  can produce an increase of the continuum emission near the H $\alpha$  line of roughly 10%, which is consistent with the observed continuum contrast in this WLF.

We should note that the estimation of the energy content of nonthermal electrons suffers from great uncertainties, mostly due to the uncertainty of the low-energy cutoff, especially when the spectrum is very steep. Sui, Holman, & Dennis (2005) constrained the low-energy cutoff to a very narrow range of  $24 \pm 2$  keV for an M1.2 solar flare by assuming thermal dominance at low energies and a smooth evolution of thermal parameters from the rise to the impulsive phase of the flare. If we take the low-energy cutoff to be 15 or 25 keV, the energy flux would rise to 6 times or drop to only 25% of the above value, respectively. The latter case could not meet the requirement of sufficient heating to account for the continuum contrast.

The observational facts that the continuum contrast reaches  $\sim$ 10% and that the HXR spectrum is very soft imply that electrons of very high energies are not the necessary condition for the generation of the continuum emission in WLFs. Nonthermal electrons of intermediate energies deposit most of their energy in the upper chromosphere, while the radiative backwarming effect plays the right role in sufficiently heating the lower chromosphere and below.

### 3.2. FOOTPOINT MOTION HISTORY

It has been recognized that the apparent HXR footpoint motion maps the successive reconnection process during solar flares. Different magnetic configurations around the flaring regions can result in different patterns of HXR footpoint motions. For example, using the *Yohkoh* HXT observations, Sakao et al. (2000) found that the double HXR footpoints move antiparallel in 7 out of the 14 flares studied. Since the launch of *RHESSI* in 2002 February, some more research has been dedicated for this topic. For example, Krucker, Hurford, & Lin (2003) found a systematic motion of one HXR footpoint nearly parallel to the magnetic neutral line in the 2002 July 23 X4.8 solar flare. Liu et al. (2004) observed an increasing separation of two HXR footpoints that is predicted by the magnetic reconnection process in the well adopted solar flare model (Kopp & Pneuman 1976).

Compared to the large number of solar flares detected in HXR, SXR, H $\alpha$ , etc., detection of WLFs is very sporadic because of the fact that WLFs represent only a small fraction of solar flares; and most importantly, the white-light continuum emission is usually constrained in a small area and limited in a time period during the impulsive phase. There are few studies on the source motion as seen in the continuum in the past decades owing to the rare detection of WLFs and the low cadence of observations. The flare under study has a relatively simple morphology in both the HXR and continuum emission, which enables us to trace and study the footpoint motion in both the two wavelengths during the flare. Comparison of the footpoint motion history in the HXR and continuum emission sheds new lights and put constraints on the modeling of WLFs.

We plot in Figure 4 the centroids of the continuum emission (*plus sign*) at the time during which ground-based observations were made, as well as the centroids of the 12–25 keV HXR emission (*diamond sign*), superposed on the MDI longitudinal magnetogram. Here the centroid refers to the intensity-weighted mean position of those parts of the source that have intensity  $\geq 50\%$  of the maximum source intensity. It is very obvious that the continuum source and the HXR source move in a similar trend: they first move westward and then turn back to the east after the maximum phase (at  $\sim 01:50:08$  UT). Meanwhile, both the westward and eastward motions are nearly parallel to the magnetic neutral line (*dashed line*). After the turnover, the source moves along a line more apart from the magnetic neutral line.

To demonstrate the relationship between the footpoint motion and the magnetic configuration of the flare, we further conduct potential field extrapolation of the MDI magnetogram using the code of Sakurai (1982), which can provide rough information about magnetic con-

nectivity around the flaring region. As shown in Figure 5, the flare is confined to a series of low-lying magnetic loops. A possible picture for the flare is as follows: first, the footpoint moves westward as a result of the successive reconnection between the low-lying magnetic loops; then, the reversal of the footpoint motion may be related to triggering of nearby larger loops more distant from the magnetic neutral line.

Since the HXR emission in 12–25 keV may contain considerable thermal contribution from the hot plasma in the flaring loop, the HXR centroid mentioned above may represent the weighted center of both the footpoint and loop top sources. However, we believe that the centroid motion is mainly from the motion of the footpoint source. For this sake, we also check the source motion in 25–50 keV, at which thick-target bremsstrahlung emission is dominant. The results show that the motion pattern is similar to what is found above during the maximum phase when the 25–50 keV HXR images are available.

Although there is a very good spatial correspondence of the continuum emission to the 12–25 HXR emission as the flare goes on, there still exists a clear offset of 2''–4'' between the centroids of the continuum and the HXR source, as shown in Figure 4. Because of the limit of spatial resolution and uncertainty of image coalignment, we cannot draw a clear conclusion whether the offset is really physical or not.

On the other hand, some studies of two-ribbon flares have shown that the nonthermal signal revealed in H $\alpha$  spectra is much more distinct at the outer edges (e.g., Canfield et al. 1993; Li & Ding 2004), where an electron beam streams down along newly reconnected lines and bombards the chromosphere. In our case, both the HXR emission and the continuum emission are found to be more apparent at the outer edges of the main flare ribbon, which is consistent with the previous results.

### 3.3. MAGNETIC RECONNECTION AT LOW ALTITUDES

Generally, magnetic reconnection and subsequent energy release in solar flares are assumed to occur in the corona. On the other hand, some active phenomena show evidence of local heating in the lower atmosphere (at chromospheric levels and below), such as the Type II WLFs and Ellerman bombs (e.g., Ding, Fang, & Yun 1999; Chen, Fang, & Ding 2001). In such cases, magnetic reconnection is assumed to take place in the lower atmosphere where the plasma is much denser and partially ionized. There is, however, no theory that can deal with the particle acceleration in the lower atmosphere. In such levels, the plasma is highly

collisional, and the energy released through magnetic reconnection is mostly consumed to ionize the plasma. Therefore, we can postulate that few particles can be accelerated to very high energies. If the accelerated electrons still follow a power-law distribution, the slope may be much steeper as compared to those cases in which reconnection occurs in the corona.

Now we discuss the details of the flare on 2002 September 30. First, there are some aspects similar to the Type A flares or Thermal Hot Flares mentioned by Tanaka (1987) and Dennis (1988): the time evolution of the HXR emission below 50 keV is very gradual and there is no visible increase of HXR emission above 50 keV; the HXR spectrum in 10–50 keV follows a nonthermal power-law with a very steep slope of  $\gamma \approx 7$ . Such features are possibly linked to a higher density at the energy release site (Dennis 1988). Second, as seen from Figure 4, the magnetic configuration and the footpoint motion imply a scenario of magnetic reconnection taking place in a series of low-lying magnetic loops during the flare. Thus, we propose that the scenario of magnetic reconnection relatively low in the atmosphere may explain the quite soft HXR spectrum observed in this flare. However, we also note that this explanation is very speculative.

Since we do not find a HXR footpoint pair from *RHESSI* images, we are unable to directly measure the loop size and altitude. By assuming semicircular loops symmetrically straddling over the magnetic neutral line, the loop altitude is roughly estimated to be the mean distance between the footpoint and the neutral line, i.e.,  $\sim 2\text{--}5''$  ( $\sim 1500\text{--}3500$  km) above the photosphere, which falls in between the upper chromosphere and the lower corona. This fact seems to support our conjecture that this flare occurs in a relative low site.

As shown in §3.2, during the maximum phase, the HXR spectrum follows a power-law that extends down to  $\sim 10$  keV and the derived energy flux of beam electrons is sufficient to account for the continuum contrast. On the other hand, since the HXR spectrum is very soft, thermal plasma may contribute largely to the HXR emission in the low energies, e.g., below  $\sim 20$  keV. We show in Figure 2 that the plasma temperature, which is derived from the background-subtracted *GOES* 0.5–4 Å and 1–8 Å SXR fluxes (e.g., Thomas, Starr, & Crannell 1985; Garcia 1994), well matches the development of the continuum emission. Matthews et al. (2003) also showed that some WLFs exhibit a stronger correlation with the SXR emission than with the HXR emission. Therefore, another possible origin of the continuum emission, i.e., thermal heating plus preferentially the backwarming effect, is worth investigating in the future.

#### 4. CONCLUSIONS

After a synthesising analysis of the WLF on 2002 September 30, we find that there is a fairly close relationship in both time and space between the continuum and the HXR emission during the flare. We discover a footpoint motion seen in the optical continuum; the motion history follows roughly that of the HXR source. This gives strong evidence that this WLF is powered by energetic electrons followed by the radiative backwarming effect. The magnetic configuration of the flaring region implies magnetic reconnection taking place at a relatively low layer during the flare. The HXR spectrum is thus very soft, possibly, due to a low efficiency of electron acceleration at low altitudes. However, the energy content of the electron beam is still enough to produce the heating in the lower atmosphere where the continuum emission originates. Radiative backwarming is of course an important mechanism to transport the energy below when direct heating is obviously impossible.

We would like to thank H. Hudson and the referee for constructive comments that help improve the paper. We are grateful to the *RHESSI*, *SOHO/MDI*, *TRACE*, and *HXRS* teams for providing the observational data and to T. Sakurai for providing the current-free magnetic extrapolation program. We thank S. Krucker for help in *RHESSI* data analysis and F. Fárník for interpreting the *HXRS* data. *SOHO* is a project of international cooperation between ESA and NASA. This work was supported by NKBRSF under grant G20000784, NSFC under grants 10025315, 10221001, and 10333040, and FANEDD under grant 200226.

#### REFERENCES

Aboudarham, J., & Hénoux, J.-C. 1987, A&A, 174, 270

Allred, J. C. Hawley, S. L., Abbott, W. P., & Carlsson, M. 2005, ApJ, 630, 573

Brown, J. C. 1971, Sol. Phys., 18, 489

Chen, P. F., Fang, C., & Ding, M. D. 2001, Chinese J. Astron. Astrophys., 2, 176

Chen, Q. R., & Ding, M. D. 2005, ApJ, 618, 537

Canfield, R. C., et al. 1993, ApJ, 411, 362

Dennis, B. R. 1988, Sol. Phys., 118, 49

Ding, M. D., Chen, Q. R., Li, J. P., & Chen, P. F. 2003a, *ApJ*, 598, 683

Ding, M. D., Fang, C., & Yun, H. S. 1999, *ApJ*, 512, 454

Ding, M. D., Liu, Y., Yeh, C.-T., & Li, J. P. 2003b, *A&A*, 403, 1151

Fang, C., & Ding, M. D. 1995, *A&AS*, 110, 99

Fárník, F., Garcia, H., & Karlický, M. 2001, *Sol. Phys.*, 201, 357

Gan, W. Q., & Mauas, P. J. D. 1994, *ApJ*, 430, 891

Garcia, H. 1994, *Sol. Phys.*, 154, 275

Handy, B. N. et al. 1999, *Sol. Phys.*, 187, 229

Huang, Y. R., Fang, C., Ding, M. D., Gao, X. F., Zhu, Z. G., Ying, S. Y., Hu, J., & Xue, Y. Z. 1995, *Sol. Phys.*, 159, 127

Hudson, H. S. 1972, *Sol. Phys.*, 24, 414

Hudson, H. S., Acton, L. W., Hirayama, T., & Uchida, Y. 1992, *PASJ*, 44, L77

Hudson, H.S., Wolfson, C. J., & Metcalf, T. R. 2005, *Sol. Phys.*, in press

Kopp, R. A., & Pneuman, G. W. 1976, *Sol. Phys.*, 50, 85

Krucker, S., Hurford, G. J., & Lin, R. P. 2003, *ApJ*, 595, 103

Li, J. P., & Ding, M. D. 2004, *ApJ*, 606, 583

Lin, R. P., et al. 2002, *Sol. Phys.*, 210, 3

Liu, W., Jiang, Y. W., Liu, S., & Petrosian, V. 2004, *ApJ*, 611, 53

Machado, M. E., et al. 1986, in *The Lower Atmosphere of Solar Flares*, ed. D.F.Neidig (Sunspot: NSO), 483

Machado, M. E., Emslie, A. G., & Avrett, E. H. 1989, *Sol. Phys.*, 124, 303

Matthews, S. A., van Driel-Gesztelyi, L., Hudson, H. S., & Nitta, N. V. 2003, *A&A*, 409, 1107

Metcalf, T. R., Alexander, D., Hudson, H. S., & Longcope, D. W. 2003, *ApJ*, 595, 483

Metcalf, T. R., Canfield, R. C., Avrett, E. H., & Metcalf, F. T. 1990a, *ApJ*, 350, 463

Metcalf, T. R., Canfield, R. C., & Saba, J. L. R. 1990b, *ApJ*, 365, 391

Neidig, D. F. 1989, *Sol. Phys.*, 121, 261

Neidig, D. F., & Kane, S. R. 1993, *Sol. Phys.*, 143, 201

Qiu, J., Lee, J., Gary, D. E., & Wang, H. 2002, *ApJ*, 565, 1335

Sakao, T., Kosugi, T., Masuda, S., & Sato, J. 2000, *Adv. Space Res.*, 26, 497

Sakurai, T. 1982, *Sol. Phys.*, 76, 301

Scherrer, P. H., et al. 1995, *Sol. Phys.*, 162, 129

Sui, L., Holman, G. D., & Dennis, B. R. 2005, *ApJ*, 626, 1102

Tanaka, K. 1987, *PASJ*, 39, 1

Thomas, R. J., Starr, R., & Crannell, C. J. 1985, *Sol. Phys.*, 95, 323

Xu, Y., Cao, W., Liu, C., Yang, G., Qiu, J., Jing, J., Denker, C., & Wang, H. 2004, *ApJ*, 607, L131

Xu, Y., Cao, W., Liu, C., Yang, G., Jing, J., Denker, C., & Wang, H. 2005, *ApJ*, submitted

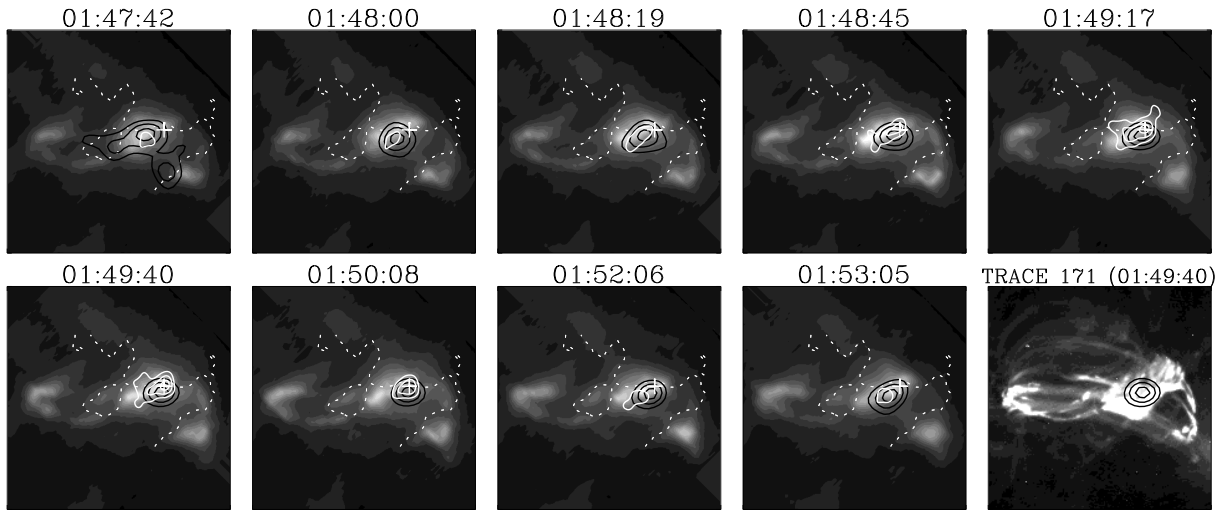


Fig. 1.— Evolution of the flare in H $\alpha$  (gray scale), continuum (white contours, with levels of 0.03, 0.06, and 0.09), and *RHESSI* 12–25 keV HXR emission (black contours, with levels of 50%, 70%, and 90% of the maximum source intensity in each image) from 01:47:42 UT to 01:53:05 UT. The *TRACE* 171 Å emission at 01:49:40 UT is also shown at the lower right panel for comparison. The white dotted line is the magnetic neutral line of the MDI magnetogram at  $\sim$ 01:36:01 UT with a correction of 14 minutes for solar rotation. The field of view is  $90'' \times 90''$ . North is up and east is to the left.

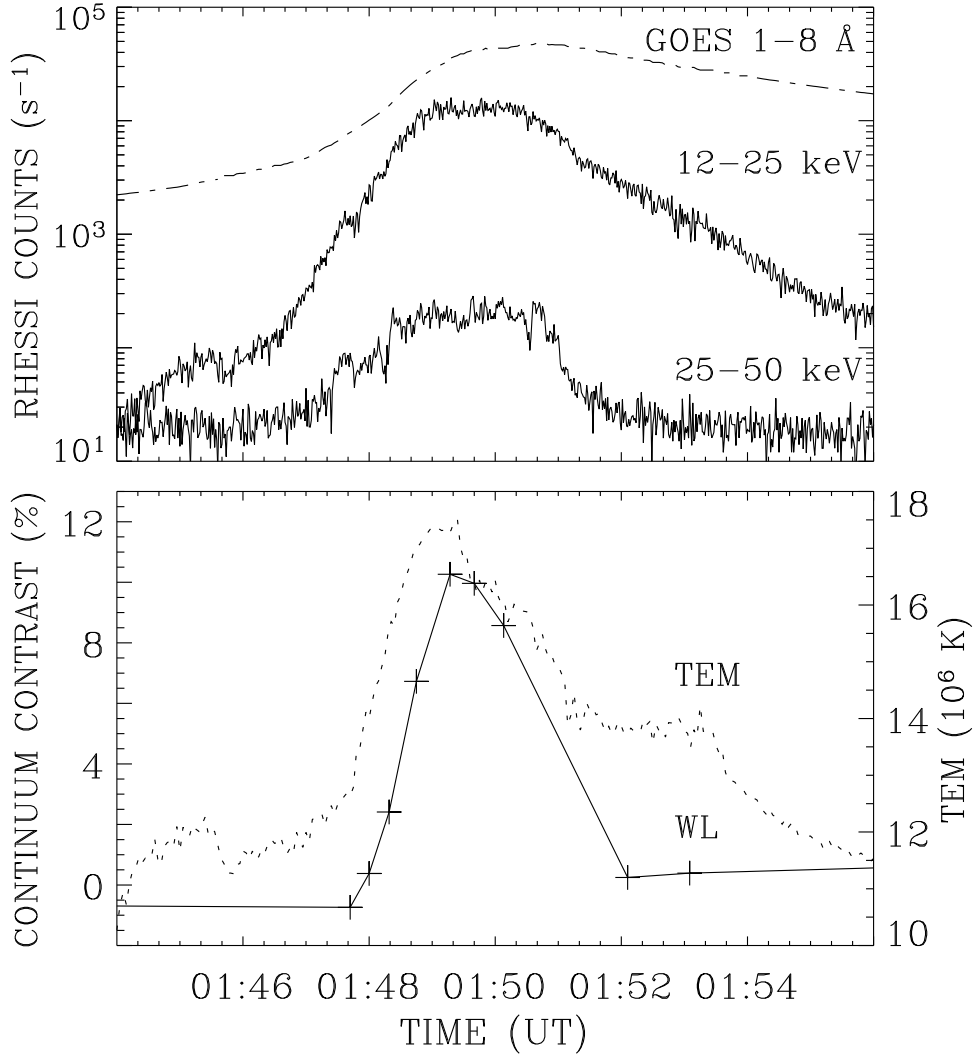


Fig. 2.— *Top panel:* Time profiles of the *RHESSI* HXR emission in 12–25 keV and 25–50 keV. Also plotted is the *GOES* 1–8 Å SXR flux in arbitrary units (*dot-dashed line*). *Bottom Panel:* Time variation of the continuum contrast at the position denoted with the *plus* (+) sign in Figure 1. The *dotted line* shows the evolution of the temperature derived from the background-subtracted *GOES* 0.5–4 Å and 1–8 Å SXR fluxes.

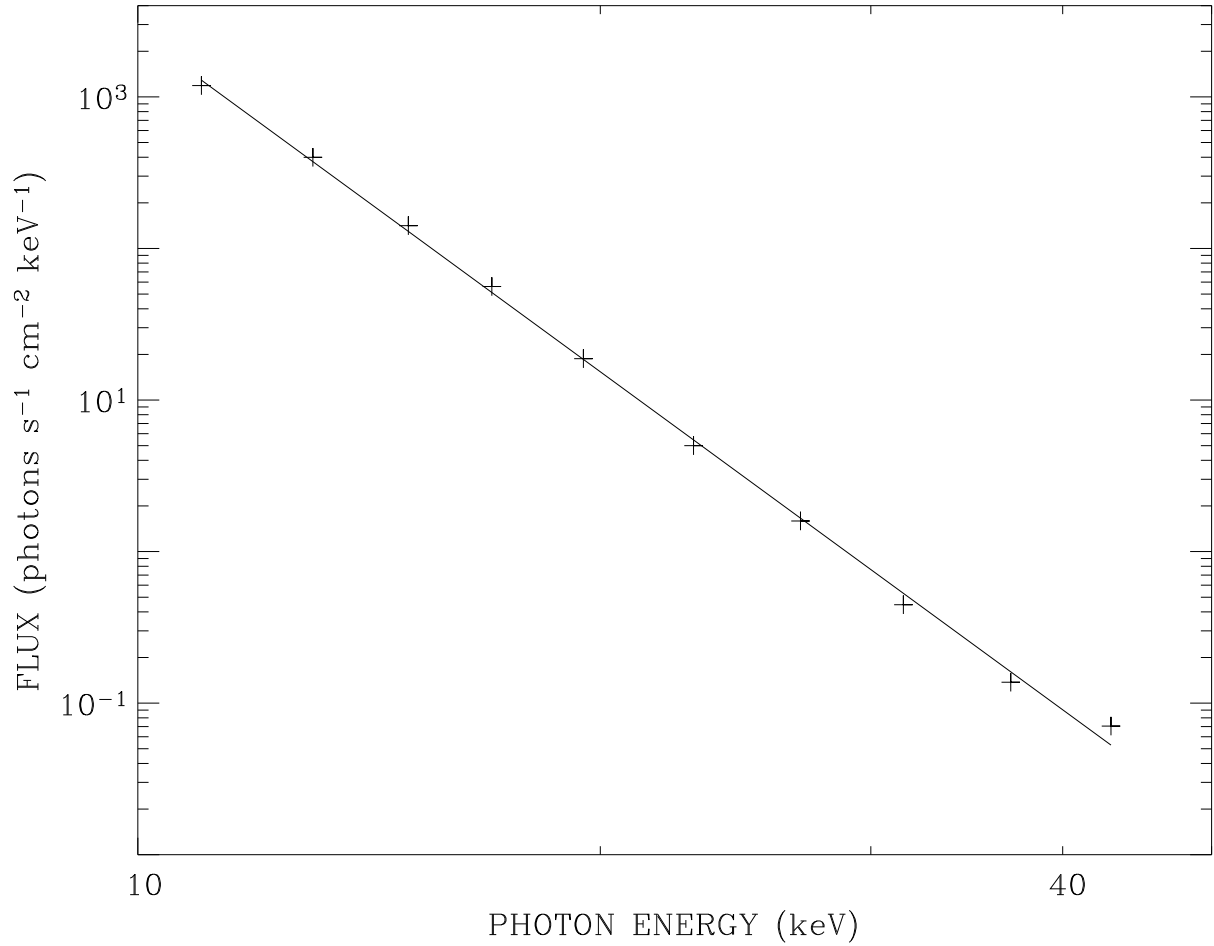


Fig. 3.— Photon spectrum and its power-law fitting for the HXR footpoint with an integration time from 01:49:00 to 01:50:00 UT. The power-law spectrum has a slope of  $-7.4$  and and a flux at 50 keV of  $\sim 1.73 \cdot 10^{-2}$  photons  $s^{-1}$   $cm^{-2}$   $keV^{-1}$ .

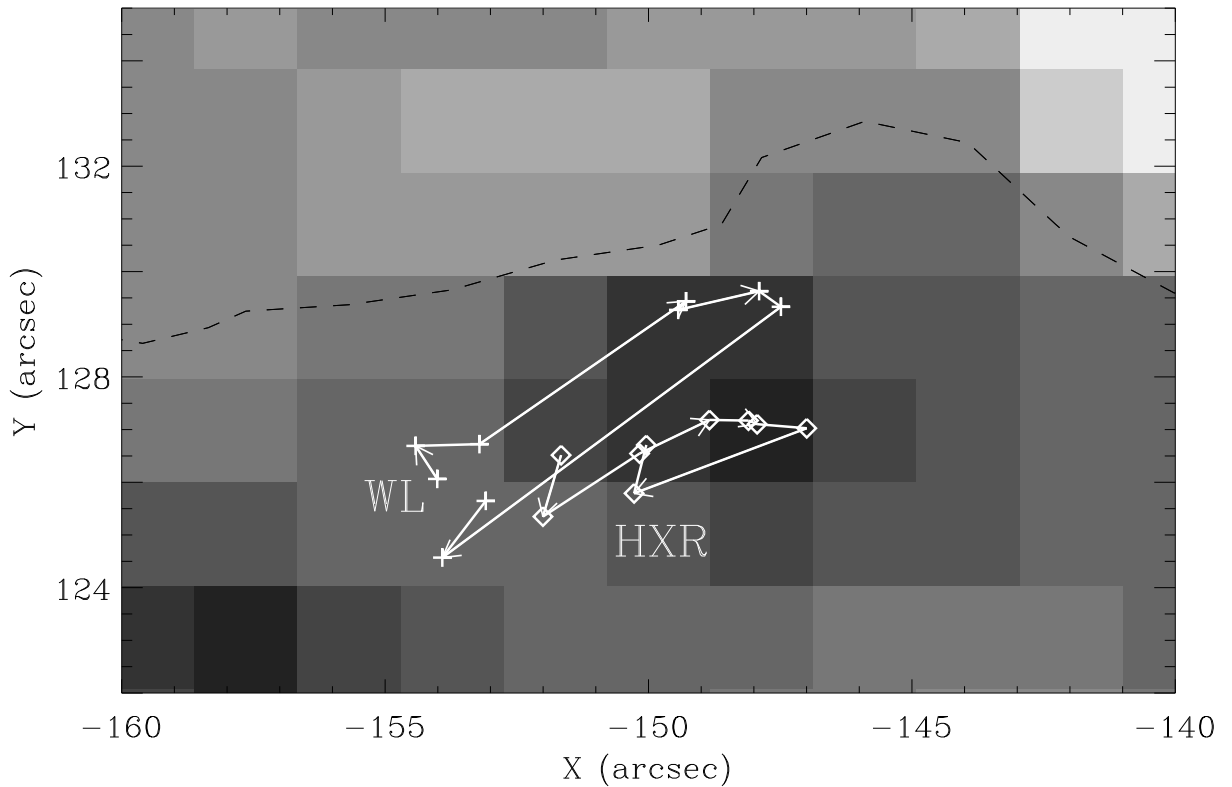


Fig. 4.— Footpoint motion history in the continuum (*plus sign*) and 12–25 HXR emission (*diamond sign*) superposed on the MDI magnetogram. The nine time points refer to those times denoted in Figure 1. The footpoint first move westward and then turns back to the east. The magnetic neutral line is plotted as *black dashed line*.

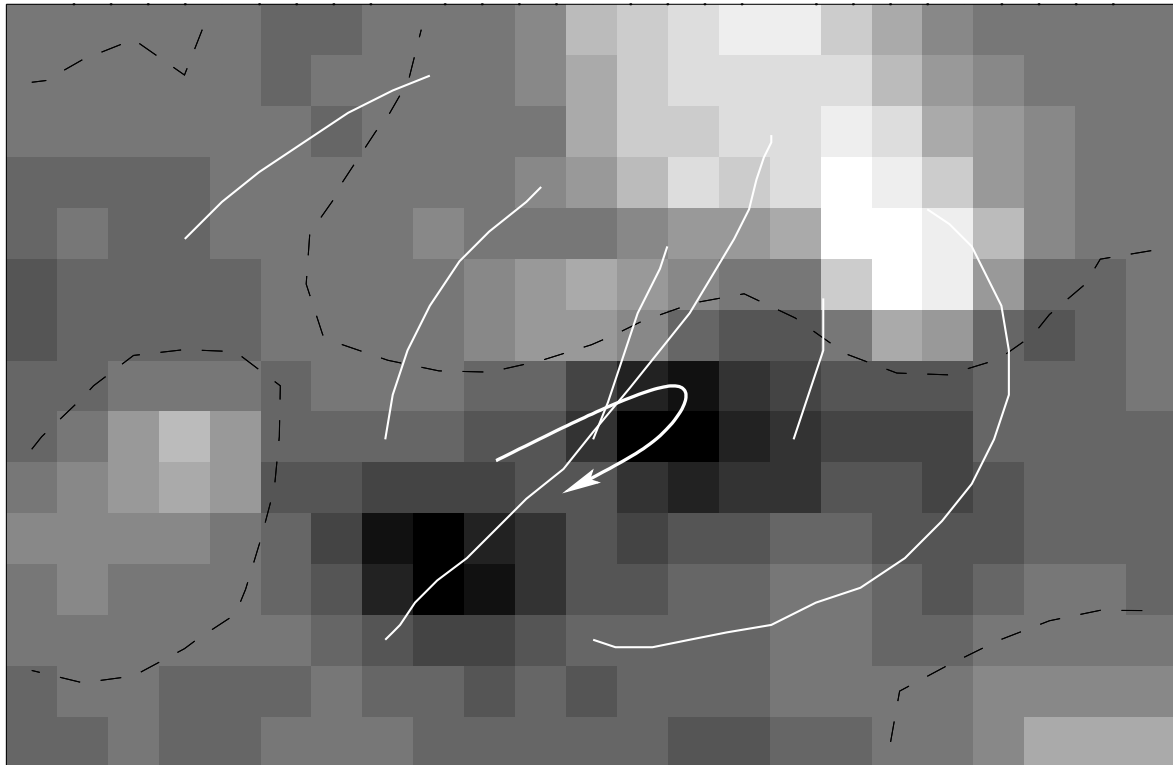


Fig. 5.— Magnetic field lines (*white solid lines*) extrapolated from the MDI longitudinal magnetogram (*gray image*). The footpoint motion trajectory, denoted as a *thick white curve*, is superposed on the magnetogram to show its relationship with the magnetic configurations around the flare. The field of view is  $45'' \times 30''$ . North is up and east is to the left.